INORGANIC CHEMISTRY FRONTIERS

RESEARCH ARTICLE

View Article Online
View Journal | View Issue

Cite this: *Inorg. Chem. Front.*, 2023, **10**, 3224

Zeolite analogues based on oxysulfidometalate supertetrahedral clusters *via* coulombic interactions†

Ming-Bu Luo,[a] Li-Jun Chen,[a] Shan-Lin Huang,[a] Xuechou Zhou,[d] Er-Xia Chen*[a,b,c] and Qipu Lin *[a,c]

Received 25th February 2023,
Accepted 23rd April 2023

DOI: 10.1039/d3qi00360d

rsc.li/frontiers-inorganic

Four zeolite-like crystalline salts, T3-MEP and T4-MTN/DIA/LON (where MEP, MTN, DIA and LON are the topological codes), have been fabricated. They are self-assemblies of anionic supertetrahedral clusters of T3-$[Sn_{10}O_4S_{20}]^{8-}$/T4-$[Sn_4In_{12}Zn_4O_4S_{31}]^{10-}$ and protonated amines by electrostatic interactions. Among them with zeotype assignment, T3-MEP has the cubic unit-cell parameter a = 50.58 Å whereas T4-MTN features cubic system axial-lengths reaching 80.44 Å. All of them present excellent proton-conductivity, *e.g.*, T3-MEP exhibits over 10^{-3} S cm^{-1} under 50 °C and 98% relative humidity.

Introduction

Microporous oxide-based zeolites are built from Si and/or Al in tetrahedral coordination and are at the center of many important industrial applications, including petrochemical refining and gas separation.[1–3] So far, over 248 types of zeolite frameworks have been registered by the Structure Commission of International Zeolite Association.[4] However, the large optical band-gap and the inherent single component characteristic of zeolites restrict their application fields. Integration of organic species and the combination of a variety of different metals into the skeleton of zeolites offer great opportunity for expanding their architectures and functionalities. Accordingly, zeolite-like metal–organic frameworks (MOFs) which are constructed using inorganic units and organic struts have been well explored.[5–8] Substitution of the classical tetrahedral Si/Al nodes by divalent metal cations such as Zn^{2+}, Co^{2+} and the oxide spacers by angular imidazolates or their derivatives in an aluminosilicate zeolite has led to one subset of MOFs, also well known as ZIFs.[9–13] Substitution of two divalent cationic centers in ZIFs by one monovalent ion and one trivalent ion, typically, Li^+ and B^{3+} respectively, generating another subset of MOFs, *viz.* BIFs.[14–17] The interconnection of tetrahedral $\{Cu_4I_4\}$ clusters and linearly ditopic molecules of diazabicyclo [2.2.2]octane ($C_6H_{12}N_2$) forms a zeotype structure denoted as COZ-1.[18] Two widely studied MOFs, MIL-100 and MIL-101, are by corner-sharing comprised of tetrahedral cages, which are defined by four chromium trimers linked by carboxylate anions, affording an MTN architecture if serving the tetrahedral cages as a 4-connected node.[19,20] Nevertheless, zeolite-like MOFs are still rare, because of the limited tetrahedrally shaped structural moieties, which are the fundamental components for zeolitic topology.

Supertetrahedral chalcogenido metalate clusters are considered to be a promising building unit in the design of zeotype frameworks due to their diverse composition and specific geometric configuration.[21–25] On account of the smaller bond angle of metal–chalcogen–metal than metal–oxygen–metal coupled with diversified coordination modes of chalcogen atoms, chalcogenido metalate clusters tend to form a pore-free architecture. Until now, most of the zeolitic nets (*viz.* SOD, BCT, ABW, RWY, NAB) composed of metal–chalcogenide clusters have been microporous, except ISC-16-MInS (M = Zn/Fe) and T3-SnOX-MTN (X = S/Se) reported recently.[26–30] Hence, construction of metal–chalcogenide clusters through self-assembly processes for the formation of periodic lattices mimicking zeolites and featuring large-pores is a daunting challenge.

In contrast to the rigid pores in extended frameworks by direct-bonding, the cavities enclosed by discrete molecular clusters held together *via* weak interactions exhibit enhanced

[a]*State Key Laboratory of Structural Chemistry, Fujian Institute of Research on the Structure of Matter, Chinese Academy of Sciences, Fuzhou, Fujian 350002, China. E-mail: exchen@fjirsm.ac.cn, linqipu@fjirsm.ac.cn*
[b]*Fujian Science & Technology Innovation Laboratory for Optoelectronic Information of China, Fuzhou, Fujian 350108, China*
[c]*State Key Laboratory of Photocatalysis on Energy and Environment, Fuzhou University, Fuzhou, 350116, China*
[d]*School of Life Sciences, Fujian Agriculture and Forestry University, Fuzhou, Fujian 350000, China*

†Electronic supplementary information (ESI) available: Detailed experimental procedures, X-ray crystallographic data and additional characterization figures. CCDC 2241505–2241508. For ESI and crystallographic data in CIF or other electronic format see DOI: https://doi.org/10.1039/d3qi00360d

flexibility and adaptability.[31–34] Their scalable nature enhances the accessibility of larger molecules and facilitates the understanding of the host–guest interactions. Introduction of surface highly valent metal ions can assist the isolation of discrete metal–chalcogenide clusters in a crystal lattice.[35] However, these molecular clusters, if only tetravalent metal cations are used, such as Sn^{4+}, prefer to spontaneously organize into a dense structure. Previously, chalcogenidometalate clusters orderly packed in a zeolite array *via* non-covalent interactions have been rarely reported, due to the existence of a large pore cavity adverse to structural stability.

Herein, we have developed four tin-based oxychalcogenides, of which one is based on T3-$[Sn_{10}O_4S_{20}]^{8-}$ with the MEP of a zeolite network (T3-MEP), another three consist of T4-$[Sn_4In_{12}Zn_4O_4S_{31}]^{10-}$ of a larger size (T4-MTN, T4-DIA and T4-LON). They are constructed from discrete supertetrahedral clusters by electrostatic forces between them and the protonated guest amines, which are used as templates and charge-balancing agents. Among them, the arrangement for T4-MTN generates a cubic unit-cell parameter of a = 80.44 Å, which presents the largest unit-cell parameters reported to date in crystalline chalcogenidometalate compounds. Both T3-MEP and T4-MTN possess a hierarchy system of extra-large pores. For the former, two pores labelled as 5^{12} and 6^25^{12} with internal diameters of 1.9 and 2.1 nm, respectively, are crosslinked by sharing their pentagonal windows. For the latter, there are also two pores interconnected *via* sharing their pentagonal windows (termed 5^{12} and 6^45^{12} with internal diameters of 1.6 and 2.4 nm, respectively). In addition, the abundant hydrogen-bonded network also gives tin-oxychalcogenides a good proton conductivity performance. In particular, the value of the representative T3-MEP exceeds 10^{-3} S cm^{-1} at 50 °C and 98% relative humidity (RH).

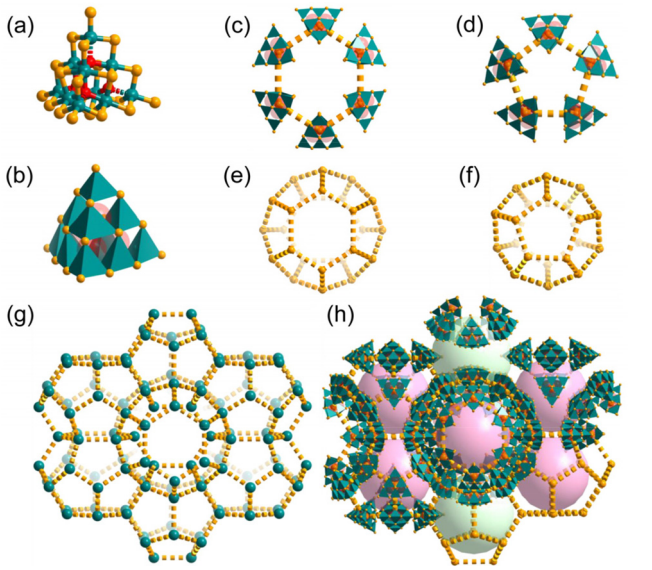

Fig. 1 Crystal structure of T3-MEP. (a and b) Discrete T3-like supertetrahedral cluster, $[Sn_{10}O_4S_{20}]^{8-}$, in ball-stick and polyhedral representation. (c and d) Hexagonal and pentagonal windows encircled by T3-clusters. (e and f) 6^25^{12} cage A and 5^{12} cage B created by connecting the centers of the supertetrahedral units. (g and h) MEP-type arrangement of the cluster anions and its MEP net topology. Sn, teal; S, gold; O, red.

Results and discussion

Colourless octadecahedral crystals of T3-MEP were prepared by mixing *n*-butyltin trichloride (^{n}BuSnCl$_3$), thiourea ($(NH_2)_2CS$), *N*-methyl-2-pyrrolidone (NMP), $SnCl_2{\cdot}2H_2O$ and La$(NO_3)_3{\cdot}6H_2O$. The mixture was sealed in a Teflon-lined stainless-steel Parr autoclave, and heated at 120 °C for 8 days. The crystals of pure phase were obtained after 3 days in room temperature. For T4 series, the solvothermal reaction of ^{n}BuSnCl$_3$, $(In(OAc)_3{\cdot}6H_2O)$, $Zn(OAc)_2{\cdot}2H_2O$, and $(NH_2)_2CS$, in the presence of different amines, heated at 120 °C for 7 days, afforded pale yellow octahedrally shaped crystals (for T4-MTN/DIA) and hexagonal prism crystals (for T4-LON). Details of the syntheses are provided in the ESI.† All members of the tin-based oxychalcogenides have been characterized by a variety of techniques (available in the ESI†).

Single-crystal X-ray diffraction (XRD) studies revealed that T3-MEP crystallizes in a cubic space group, $Pm\bar{3}n$, with lattice parameters a = 50.584 Å, V = 129 431 Å^3. As shown in Fig. 1a, there are two types of Sn atoms. Each of the four apex Sn atoms bonds with four S atoms and one O atom adopts a trigonal-bipyramidal geometry, and the remaining Sn atoms on the edges are octahedrally coordinated by four S and two O atoms. Its unit-cell contains 46 supertetrahedral oxygen-stuffed stannate cluster anions of $\{Sn_{10}O_4S_{20}\}^{8-}$, which are charge balanced by H$^+$NMP cations. The counterions and other organic species in the cluster-based chalcogenidometalate structures are hard to be identified by XRD, but the co-crystallization of H$^+$NMP in T3-MEP could be detected by mass spectrometry (MS) (Fig. S1†). To accommodate the charge balance, there are eight H$^+$NMP cations per cluster. Some of the H$^+$NMP cations may be located between two clusters with their rings oriented parallel to the faces of the cluster, which can be seen in the electron density difference map (Fig. S6†). The contribution of the highly disordered H$^+$NMP and other solvate molecules was removed from the reflection data using the SQUEEZE procedure. Every two adjacent clusters are almost face-to-face parallel with an interplanar distances of *ca.* 5.5 Å (Fig. S7†). The H$^+$NMP cations provide T3-MEP with a strong electrostatic effect, which induces $\{Sn_{10}O_4S_{20}\}^{8-}$ anions to be scattered in 3D space to form a MEP net where each cluster is simplified as a node. Notably, the MEP topology is uncommon, and only one case of MPF-1 in MOFs has been reported so far.[36] Accordingly, T3-MEP can be divided into two categories of windows of five- and six-membered rings with aperture sizes of *ca.* 1.1 and 1.6 nm, and two categories of cages: cage-A composed of 24 and cage-B composed of 20 cluster units (Fig. 1e and f, marked as 6^25^{12} and 5^{12}), with diameters of about 2.1 and 1.9 nm, respectively, following consideration of the van der Waals radius of the edge atoms. Each cage-A is

surrounded by 10 cages-A through face-sharing of two hexagonal rings and eight pentagonal rings, and connects to 4 cages-B through face-sharing of the pentagonal rings (Fig. S9†). To the best of our knowledge, such giant cages are still rare in cluster-based metallic chalcogenides, and even in MOFs.[37–41] As calculated by PLATON, the solvent available volume is ~73% of the entire crystal volume.

T4-MTN is of sulfido-oxido stannate zeotype network based on $\{Sn_4In_{12}Zn_4O_4S_{31}\}^{10-}$ cluster anions of larger version than ones in T3-MEP. Accordingly, compared with T3-MEP, T4-MTN has larger cubic unit cell parameters of a = 80.44 Å, which surpasses the series of T3-MTN recently reported by us, and also represents the largest lattice parameters for all of the chalcogenidometalate crystals. In the structure of T4-MTN, the two opposite triangular faces from two different adjacent clusters are nearly parallel (dihedral angles, 0° and 8°) in an eclipsed configuration with the interplanar spacing of *ca.* 6.3 Å (Fig. S7†). In addition to the same 5^{12} cages as in T3-MEP, T4-MTN contains larger hexadecahedral cages, termed $6^4 5^{12}$ (Fig. S11†). The diameters of the spherical cavities within 5^{12} and $6^4 5^{12}$ cages are *ca.* 1.6 nm and 2.4 nm, respectively (taking into account the van der Waals radius of the protruding atoms). Its extra-cluster volume ratio is 64.8% as estimated by PLATON.

By using different protonated amines as counterions and templates, three other zeolite-like four-connection networks, *i.e.*, T4-DIA, T4-LON and T4-SOD[42] (T4-SOD was reported by Wu *et al.*), based on the similar discrete T4 cluster as that of T4-MTN can be obtained (Fig. 2). T4-DIA crystallizes in a pretty common diamond-topology net, which is the underlying structure for the assembly of tetrahedral nodes. All the opposite faces of adjacent clusters in T4-DIA are arranged in a parallel and staggered fashion with an interplanar distance of *ca.* 7 Å. Within T4-DIA, a 6^4 cage with a diameter of ~8.4 Å was formed (Fig. S12†). The lonsdaleite-topology in T4-LON is quite similar to the diamond network but relatively rare. For T4-LON, the clusters are packed to form both boat-like and chair-like six-membered rings, which together generate an ultrasmall 6^5 cage of 6.6 Å in diameter (Fig. S13†). Different from the stacking patterns above, in T4-SOD, the two opposite trigonal faces of neighbouring clusters adopt a non-parallel fashion, resulting in a distorted truncated octahedral cage with a twist of a square ring and a hexagonal ring, eventually forming a sodalite net (Fig. S14†).

The electronic structures of these cluster-based zeotype networks were investigated by diffuse reflectance UV-vis spectroscopy. The results indicate that the packing pattern has less impact on its absorption edge, while the size of the cluster significantly affects its bandgap. As shown in Fig. S21,† T3-MEP has a bandgap of *ca.* 3.16 eV, much greater than that of the chalcogenidometalate compounds based on T4 clusters, ranging from 2.68 eV to 2.45 eV estimated by the Kubelka–Munk function.[43,44] This could be mainly attributed to the size dependent effect relative to its energy band structure. Thermogravimetric analysis reveals that the packing arrangement is a critical factor affecting its stability. Among them, T4-DIA was observed to have the highest thermal decomposition

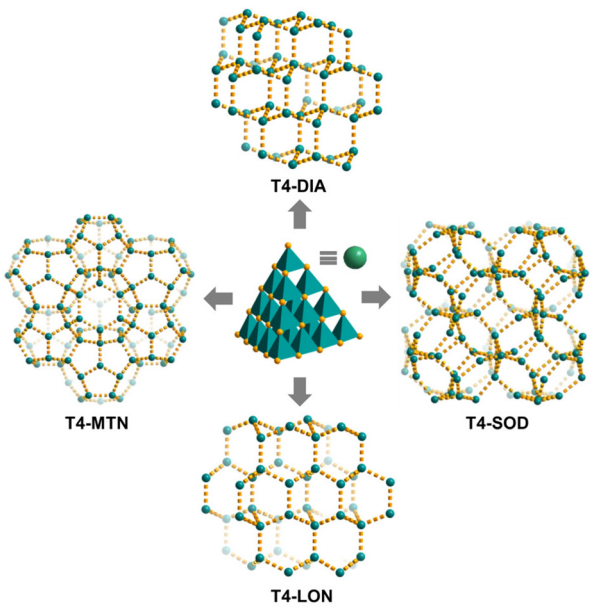

Fig. 2 (a) Different topological nets constructed by treating discrete T4-type supertetrahedral clusters as a node.

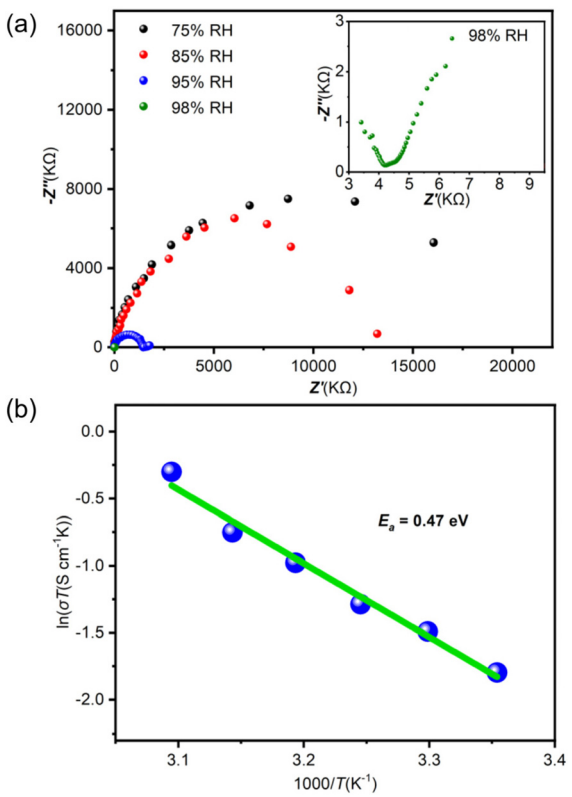

Fig. 3 (a) Nyquist plots of the pelleted sample of T3-MEP at different RH at 25 °C. (b) Arrhenius plots of proton conductivity *vs.* the temperature for T3-MEP under 98% RH.

temperature (up to 180 °C), due to the compact stacking of clusters and the strong electrostatic forces between clusters and protonated amines.

The existence of the abundant H^+-carriers suggests the possibility of using these zeotype-lined chalcogenides based on clusters as hydrated proton conductors. As a representative, the Nyquist plots of T3-MEP were obtained by subjecting the compacted pellets to alternating-current impedance spectroscopy to evaluate its proton-conductivity under varying relative humidities (RH, 75–98%) at 25 °C (Fig. 3a). The proton-conductivity is positively associated with RH. As the RH increases from 75% to 98%, the conductivity gradually increases from 1.32×10^{-7} to 5.56×10^{-4} S cm^{-1}. To further understand the conducting mechanism, the dependence of conductivity on temperature was investigated at 98% RH (Fig. 3b), and the proton conductivity of T3-MEP reached 2.29×10^{-3} S cm^{-1} at 50 °C. As determined from the Arrhenius plot, its activation energy (E_a) is 0.47 eV. The high activation energy indicates that the proton carrier transfer follows the vehicle mechanism.

Conclusions

In conclusion, four zeolite analogues of sulfido-oxido stannate crystal salts have been prepared, *viz*. T3-MEP and T4-MTN/DIA/LON based on tetrahedrally shaped clusters, T3-$\{Sn_{10}O_4S_{20}\}^{8-}$ or T4-$\{Sn_4In_{12}Zn_4O_4S_{31}\}^{10-}$, respectively. These clusters are charge-complemented by protonated organic amines. Under the assistance of coulombic interactions, such oxide-filled clusters are distributed in 3D space to develop four 4-connected topological networks (MEP, MTN, DIA, and LON). Among them, T4-MTN exhibits a cubic unit-cell of 520 446 Å^3, which is the largest in the family of the crystalline cluster-based metal–chalcogenides. Similar to the T4-MTN made of cages 5^{12} and 6^45^{12} with diameters of 1.6 and 2.4 nm, T3-MEP has hierarchically colossal cavities, *viz*. cages 5^{12} and 6^25^{12} of diameters of 1.9 and 2.1 nm. Due to the presence of abundant proton carriers, T3-MEP has a proton conductivity of 2.29×10^{-3} S cm^{-1} at 50 °C and 98% RH. This work expands zeolite-like materials composed of discrete supertetrahedral chalcogenido metalate clusters.

Author contributions

M. Luo carried out the Experimental sections and wrote the manuscript. E. Chen and Q. Lin supervised the study and reviewed the manuscript. L. Chen, S. Huang and X. Zhou, helped in the characterization. All the authors discussed the results and contributed to the manuscript.

Conflicts of interest

There are no conflicts to declare.

Acknowledgements

This research was supported by the National Key Research and Development Project (Grant No. 2022YFA1503900), the National Science Foundation of China (Grant No. 22201283), the National Science Foundation of Fujian Province (Grant No. 2022J05090), the Open Project Program of the State Key Laboratory of Photocatalysis on Energy and Environment (Grant No. SKLPEE-KF202204, Fuzhou University), and the Fujian Science & Technology Innovation Laboratory for Optoelectronic Information of China (Grant No. 2021ZR138).

Notes and references

1 M. Shamzhy, M. Opanasenko, P. Concepción and A. Martínez, New trends in tailoring active sites in zeolite-based catalysts, *Chem. Soc. Rev.*, 2019, **48**, 1095–1149.
2 L.-H. Chen, M.-H. Sun, Z. Wang, W. Yang, Z. Xie and B.-L. Su, Hierarchically Structured Zeolites: From Design to Application, *Chem. Rev.*, 2020, **120**, 11194–11294.
3 W. Fan and M. Dong, Regulation of zeolite particle morphology, *Science*, 2022, **375**, 29–29.
4 **https://www.iza-structure.org/databases/**.
5 M. Eddaoudi, D. F. Sava, J. F. Eubank, K. Adil and V. Guillerm, Zeolite-like metal–organic frameworks (ZMOFs): design, synthesis, and properties, *Chem. Soc. Rev.*, 2015, **44**, 228–249.
6 Y.-X. Tan, F. Wang and J. Zhang, Design and synthesis of multifunctional metal–organic zeolites, *Chem. Soc. Rev.*, 2018, **47**, 2130–2144.
7 F.-Y. Yi, H. Yang, X. Zhao, P. Feng and X. Bu, Zeolite-Type Metal Oxalate Frameworks, *Angew. Chem., Int. Ed.*, 2019, **58**, 2889–2892.
8 L.-D. Lin, D. Zhao, X.-X. Li and S.-T. Zheng, Recent Advances in Zeolite-like Cluster Organic Frameworks, *Chem. – Eur. J.*, 2019, **25**, 442–453.
9 H. Wang, X. Pei, M. J. Kalmutzki, J. Yang and O. M. Yaghi, Large Cages of Zeolitic Imidazolate Frameworks, *Acc. Chem. Res.*, 2022, **55**, 707–721.
10 P. Kukkar, K.-H. Kim, D. Kukkar and P. Singh, Recent advances in the synthesis techniques for zeolitic imidazolate frameworks and their sensing applications, *Coord. Chem. Rev.*, 2021, **446**, 214109.
11 J.-P. Zhang, Y.-B. Zhang, J.-B. Lin and X.-M. Chen, Metal Azolate Frameworks: From Crystal Engineering to Functional Materials, *Chem. Rev.*, 2012, **112**, 1001–1033.
12 K. S. Park, Z. Ni, A. P. Côté, J. Y. Choi, R. Huang, F. J. Uribe-Romo, H. K. Chae, M. O'Keeffe and O. M. Yaghi, Exceptional chemical and thermal stability of zeolitic imidazolate frameworks, *Proc. Natl. Acad. Sci. U. S. A.*, 2006, **103**, 10186–10191.
13 X.-C. Huang, Y.-Y. Lin, J.-P. Zhang and X.-M. Chen, Ligand-Directed Strategy for Zeolite-Type Metal–Organic Frameworks: Zinc(II) Imidazolates with Unusual Zeolitic Topologies, *Angew. Chem., Int. Ed.*, 2006, **45**, 1557–1559.

14 H.-X. Zhang, F. Wang, H. Yang, Y.-X. Tan, J. Zhang and X. Bu, Interrupted Zeolite LTA and ATN-Type Boron Imidazolate Frameworks, *J. Am. Chem. Soc.*, 2011, **133**, 11884–11887.
15 J. Zhang, T. Wu, C. Zhou, S. Chen, P. Feng and X. Bu, Zeolitic Boron Imidazolate Frameworks, *Angew. Chem., Int. Ed.*, 2009, **48**, 2542–2545.
16 Q. Hong, W. Wang, S. Chen, K. Chen, M. Liu, H.-X. Zhang and J. Zhang, Host–Guest Pore Space Partition in a Boron Imidazolate Framework for Ethylene Separation, *Chem. Mater.*, 2022, **34**, 307–313.
17 M.-Y. Bi, Y.-H. Wen, H.-X. Zhang and J. Zhang, Syntheses, Crystal Structures and Properties of Two New Zn Based Boron Imidazolate Frameworks, *Chin. J. Struct. Chem.*, 2021, **40**, 865–870.
18 Y. Kang, F. Wang, J. Zhang and X. Bu, Luminescent MTN-Type Cluster–Organic Framework with 2.6 nm Cages, *J. Am. Chem. Soc.*, 2012, **134**, 17881–17884.
19 G. Férey, C. Mellot-Draznieks, C. Serre, F. Millange, J. Dutour, S. Surblé and I. Margiolaki, A Chromium Terephthalate-Based Solid with Unusually Large Pore Volumes and Surface Area, *Science*, 2005, **309**, 2040.
20 G. Férey, C. Serre, C. Mellot-Draznieks, F. Millange, S. Surblé, J. Dutour and I. Margiolaki, A Hybrid Solid with Giant Pores Prepared by a Combination of Targeted Chemistry, Simulation, and Powder Diffraction, *Angew. Chem., Int. Ed.*, 2004, **43**, 6296–6301.
21 T. Wu, R. Khazhakyan, L. Wang, X. Bu, S.-T. Zheng, V. Chau and P. Feng, Three-Dimensional Covalent Co-Assembly between Inorganic Supertetrahedral Clusters and Imidazolates, *Angew. Chem., Int. Ed.*, 2011, **50**, 2536–2539.
22 X. Xu, W. Wang, D. Liu, D. Hu, T. Wu, X. Bu and P. Feng, Pushing up the Size Limit of Metal Chalcogenide Supertetrahedral Nanocluster, *J. Am. Chem. Soc.*, 2018, **140**, 888–891.
23 H. Yang, J. Zhang, M. Luo, W. Wang, H. Lin, Y. Li, D. Li, P. Feng and T. Wu, The Largest Supertetrahedral Oxychalcogenide Nanocluster and Its Unique Assembly, *J. Am. Chem. Soc.*, 2018, **140**, 11189–11192.
24 J. Tang, X. Wang, J. Zhang, J. Wang, W. Yin, D.-S. Li and T. Wu, A chalcogenide-cluster-based semiconducting nanotube array with oriented photoconductive behavior, *Nat. Commun.*, 2021, **12**, 4275.
25 J. Zhang, X. Bu, P. Feng and T. Wu, Metal Chalcogenide Supertetrahedral Clusters: Synthetic Control over Assembly, Dispersibility, and Their Functional Applications, *Acc. Chem. Res.*, 2020, **53**, 2261–2272.
26 W. Wang, X. Wang, D. Hu, H. Yang, C. Xue, Z. Lin and T. Wu, An Unusual Metal Chalcogenide Zeolitic Framework Built from the Extended Spiro-5 Units with Supertetrahedral Clusters as Nodes, *Inorg. Chem.*, 2018, **57**, 921–925.
27 C. Xue, D. Hu, Y. Zhang, H. Yang, X. Wang, W. Wang and T. Wu, Two Unique Crystalline Semiconductor Zeolite Analogues Based on Indium Selenide Clusters, *Inorg. Chem.*, 2017, **56**, 14763–14766.
28 N. Zheng, X. Bu, B. Wang and P. Feng, Microporous and Photoluminescent Chalcogenide Zeolite Analogs, *Science*, 2002, **298**, 2366.
29 C. L. Cahill and J. B. Parise, Synthesis and Structure of $MnGe_4S_{10}\cdot(C_6H_{14}N_2)\cdot 3H_2O$: A Novel Sulfide Framework Analogous to Zeolite Li-A(BW), *Chem. Mater.*, 1997, **9**, 807–811.
30 M.-B. Luo, S.-L. Huang, H.-D. Lai, J. Zhang and Q. Lin, Tin-oxychalcogenide supertetrahedral clusters maintained in a MTN zeolite-analog arrangement by coulombic interactions, *Chem. Commun.*, 2020, **56**, 8388–8391.
31 W.-W. Xiong, J.-R. Li, B. Hu, B. Tan, R.-F. Li and X.-Y. Huang, Largest discrete supertetrahedral clusters synthesized in ionic liquids, *Chem. Sci.*, 2012, **3**, 1200–1204.
32 E. Dornsiepen, F. Dobener, S. Chatterjee and S. Dehnen, Controlling the White-Light Generation of $[(RSn)_4E_6]$: Effects of Substituent and Chalcogenide Variation, *Angew. Chem., Int. Ed.*, 2019, **58**, 17041–17046.
33 B. Peters, G. Stuhrmann, F. Mack, F. Weigend and S. Dehnen, Highly Soluble Supertetrahedra upon Selective Partial Butylation of Chalcogenido Metalate Clusters in Ionic Liquids, *Angew. Chem., Int. Ed.*, 2021, **60**, 17622–17628.
34 N. W. Rosemann, J. P. Eußner, A. Beyer, S. W. Koch, K. Volz, S. Dehnen and S. Chatterjee, A highly efficient directional molecular white-light emitter driven by a continuous-wave laser diode, *Science*, 2016, **352**, 1301.
35 T. Wu, X. Wang, X. Bu, X. Zhao, L. Wang and P. Feng, Synthetic Control of Selenide Supertetrahedral Clusters and Three-Dimensional Co-assembly by Charge-Complementary Metal Cations, *Angew. Chem., Int. Ed.*, 2009, **48**, 7204–7207.
36 W. Zhang, K. Wang, J. Li, Z. Lin, S. Song, S. Huang, Y. Liu, F. Nie and Q. Zhang, Stabilization of the Pentazolate Anion in a Zeolitic Architecture with $Na_{20}N_{60}$ and $Na_{24}N_{60}$ Nanocages, *Angew. Chem., Int. Ed.*, 2018, **57**, 2592–2595.
37 P. Li, N. A. Vermeulen, C. D. Malliakas, D. A. Gómez-Gualdrón, A. J. Howarth, B. L. Mehdi, A. Dohnalkova, N. D. Browning, M. O'Keeffe and O. K. Farha, Bottom-up construction of a superstructure in a porous uranium-organic crystal, *Science*, 2017, **356**, 624.
38 S. M. Humphrey, J.-S. Chang, S. H. Jhung, J. W. Yoon and P. T. Wood, Porous Cobalt(II)–Organic Frameworks with Corrugated Walls: Structurally Robust Gas-Sorption Materials, *Angew. Chem., Int. Ed.*, 2007, **46**, 272–275.
39 Z. Chen, K. O. Kirlikovali, P. Li and O. K. Farha, Reticular Chemistry for Highly Porous Metal–Organic Frameworks: The Chemistry and Applications, *Acc. Chem. Res.*, 2022, **55**, 579–591.
40 G. A. Leith, C. R. Martin, K. C. Park and N. B. Shustova, Playing "Jenga" with MOFs: De-interpenetration for pore opening, *Chem*, 2022, **8**, 325–326.
41 R.-B. Lin, Z. Zhang and B. Chen, Achieving High Performance Metal–Organic Framework Materials

through Pore Engineering, *Acc. Chem. Res.*, 2021, **54**, 3362–3376.
42 C. Xue, L. Zhang, X. Wang, D. Hu, X.-L. Wang, J. Zhang, R. Zhou, D.-S. Li, H. Su and T. Wu, Enhanced Water Dispersibility of Discrete Chalcogenide Nanoclusters with a Sodalite-Net Loose-Packing Pattern in a Crystal Lattice, *Inorg. Chem.*, 2020, **59**, 15587–15594.
43 J. Tauc, R. Grigorovici and A. Vancu, Optical Properties and Electronic Structure of Amorphous Germanium, *Phys. Status Solidi*, 1966, **15**, 627–637.
44 E. A. Davis and N. F. Mott, Conduction in non-crystalline systems V. Conductivity, optical absorption and photoconductivity in amorphous semiconductors, *Philos. Mag.*, 1970, **22**, 0903–0922.